

Electrochemical Analysis of an Anode-Supported SOFC

Shuangqiao Yang, Tao Chen, Ying Wang, Zhenbo Peng, Wei Guo Wang *

Division of Fuel cell and Energy Technology, Ningbo Institute of Material Technology & Engineering, Chinese Academy of Sciences, 519 Zhuangshi Road, Ningbo 315201, China

*E-mail: wgwang@nimte.ac.cn

Received: 20 December 2012 / Accepted: 9 January 2013 / Published: 1 February 2013

Anode-supported SOFCs have received increased attention in recent years. An electrochemical model was developed and verified for a $10 \times 10 \text{ cm}^2$ anode-supported SOFC. The activation, ohmic and concentration overpotentials were taken into account in the model. The structural and operating parameters were analyzed to improve the cell design. The simulation results showed that the activation overpotential and the ohmic overpotential were responsible for most of the voltage loss. The TPB length can significantly influence the activation overpotential. An increase in porosity resulted in an increased the activation overpotential; however, the concentration overpotential decreased. The combined effects resulted in good cell performance at porosity values of 0.2 and 0.4. The thickness of the electrolyte was the dominant factor in determining the ohmic overpotential. The concentration overpotential was primarily influenced by the anode thickness. A decrease in the electrolyte and anode thicknesses improved the cell performance. Increases in the operating temperature and pressure resulted in decreased activation and concentration overpotentials, which, in turn, resulted in enhanced cell performance.

Keywords: Solid oxide fuel cell; Electrochemical model; Overpotential.

1. INTRODUCTION

Solid oxide fuel cells (SOFCs) have attracted significant attention over the past decade because of their high efficiency and the fact that they do not represent an environmental hazard [1-8]. The state-of-the-art SOFC geometries can be classified as planar and tubular [9]. Although research on tubular SOFCs has resulted in significant progress in recent years, the low power density of SOFCs due to long current paths has limited their development and application [10]. In contrast, SOFCs in a planar configuration can reach very high power density. Two main types of planar SOFCs exist: electrolyte-supported and electrode-supported. In the electrolyte-supported design, the electrolyte layer is the thickest component, which results in high ohmic resistance. In the electrode-supported design, either the anode or the cathode is the thickest component. However, cathode-supported SOFCs have a

greater activation overpotential than anode-supported SOFCs. Thus, the anode-supported SOFCs have received more attention in recent years.

The processes that influence the performance of a SOFC are complex. The use of experiments to investigate SOFCs is expensive and time consuming. If some results and key parameters can be obtained from experiments, a relatively accurate model can be constructed based on these data, and the performance of SOFCs can be subsequently analyzed using the model. A verified model offers both a better understanding of the cell and a useful tool to improve the cell performance.

All SOFC models require accurate predictions of current–voltage (I–V) curves [11]. To reach this objective, electrochemical models should be developed to characterize the overpotentials of SOFCs. The performance of an SOFC is mainly affected by activation, ohmic, and concentration overpotentials.

The activation overpotential originates from the irreversibility of the electrochemical reaction. Usually, the activation overpotential is calculated by solving the Butler–Volmer equation or some explicit empirical equation. In practice, another important parameter, the three-phase boundary (TPB) length, which has often been neglected or lumped into the exchange current density parameter, was found by Janardhanan et al. [12] and Kim et al. [13] to also significantly influence the activation. The TPB length is mainly affected by the microstructure of the electrodes. Numerous models for calculating the TPB length have been developed [14–16]. A random sphere model is an effective means to calculate the TPB length and is adopted here. Ohmic overpotential is generated by the ionic and electronic charge-transfer resistances. This parameter is important in all types of cells and is essentially linear and proportional to the current density. Concentration overpotential is generated by mass transport in the electrodes. It is often neglected due to the high gas diffusion rate at high temperatures [17–19]. However, in studies of thick anodes, such as that of Shi et al. [20], it must be considered.

High SOFC performance relies on optimum electrochemical reactions and mass transport processes. For an anode-supported SOFC, although the ohmic loss is smaller than that in other types of SOFC cells, the activation and concentration overpotentials have been reported to often outweigh the benefit of reduced ohmic losses [21]. These SOFC overpotentials are strongly affected by structural parameters, such as the thickness and porosity of the electrode, and by operating parameters, such as pressure and temperature. These parameters should be taken into account to improve the design of SOFCs.

Above all, a detailed electrochemical model is needed to enable the analysis of the activation, concentration and ohmic overpotentials.

2. EXPERIMENT

Commercial Ni-YSZ anode-supported SOFCs were acquired from the Ningbo Institute of Material Technology and Engineering (NIMTE), Chinese Academy of Sciences. The dimensions of the cells were $10 \times 10 \text{ cm}^2$. A $400 \text{ }\mu\text{m}$ thick Ni/8YSZ anode substrate was prepared by tape casting, as were the other cell layers, including a $10 \text{ }\mu\text{m}$ thick anode functional layer and a $10 \text{ }\mu\text{m}$ thick 8YSZ

electrolyte layer. The cathode of the cell was a double LSM layer sprayed onto the anode substrate before it was co-sintered. The cells were tested in an alumina testing chamber. Platinum and nickel foils were used as current collectors at the cathode and anode sides, respectively. Silver mesh sandwiched between LSM was utilized for gas distribution at the cathode side; the silver mesh was intended to decrease the contact resistance between the cathode and the current collector. For the anode side, two layers of nickel foam were used for gas distribution and current collection. Details on the testing facility are described elsewhere [22,23].

Air and humidity hydrogen were introduced into the cathode and anode, respectively. The operating temperatures were 750°C, 800°C and 850°C. The flow rate of hydrogen was 25 sccm, and the air flow rate was 62.5 sccm. After the cell tests, microstructural scanning electron microscopy (SEM) observations were performed using a HITACHI S4800 scanning electron microscope. Fig. 1 shows the SEM micrograph of a tested SOFC.

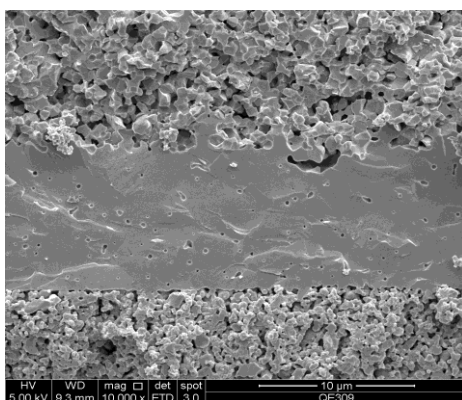


Figure 1. SEM micrograph of a tested SOFC cross-section showing (from top to bottom) the anode active layer, the electrolyte and the cathode active layer

3. MODELING

Several assumptions were made before the model was developed because of the complexity of the physical and chemical transformations that occur in SOFCs:

- 1) The flowing gases were assumed to behave as ideal gases in both the fuel and air channels.
- 2) The air was assumed to be composed of 21% oxygen and 79% nitrogen.
- 3) The temperature was assumed to be uniform in the PEN; thus, the model was assumed to be isothermal.
- 4) The pressure drop in the SOFC was neglected.

Fuels and air are fed to the anode and cathode, respectively. At the cathode, oxygen receives electrons to form oxygen ions. At the anode, fuels react with the oxygen ions to generate steam and electrons. The flow of electrons to the cathode through an external circuit produces direct-current electricity.

3.1 Actual voltage

The difference between the thermodynamic potentials of the electrode reactions determines the reversible cell voltage, which is also known as the electromotive force (emf). The emf depends on the gas composition and on the temperature at the electrodes, which can be expressed by the Nernst equation:

$$V_{\text{nerst}} = E^0 + \frac{RT}{2F} \ln\left(\frac{P_{\text{H}_2} P_{\text{O}_2}^{0.5}}{P_{\text{H}_2\text{O}}}\right) \quad (1)$$

where P_i is the partial pressure of component i . The E^0 is the open-circuit voltage and is a function of the operating temperature; it can be expressed by the following equation [24,25]:

$$E^0 = 1.253 - 2.4516 \times 10^{-4} T \quad (2)$$

This voltage is the maximum voltage that can be achieved when no electrical current is flowing through the fuel cell. For a cell, the actual voltage is lower than the open-circuit voltage because of internal resistances and overpotential losses.

The output voltage of the SOFC can be expressed as

$$V = V_{\text{nerst}} - (\eta_{\text{act}} + \eta_{\text{ohm}} + \eta_{\text{conc}}) \quad (3)$$

where η_{act} , η_{ohm} and η_{conc} are the activation overpotential, the ohmic overpotential and the concentration overpotential, respectively.

3.2 Activation overpotential

Activation polarization is associated with overcoming the reaction energy barriers at the electrode–electrolyte interface. Usually, the activation overpotential is solved using the Butler–Volmer equation, which is expressed as

$$j = j_0 \left(\exp\left(\alpha \frac{nF\eta_{\text{act}}}{RT}\right) - \exp\left(- (1-\alpha) \frac{nF\eta_{\text{act}}}{RT}\right) \right) \quad (4)$$

Noren and Hoffman [26] compared several types of explicit approximations and recommended the hyperbolic sine approximation duo because of its accuracy. The activation overpotential can therefore be written as

$$\eta_{\text{act}} = \frac{RT}{\alpha nF} \sinh^{-1}\left(\frac{j}{2j_0}\right) \quad (5)$$

where α is the symmetrical coefficient (=0.5), n is the number of electrons, and j_0 is the electrode exchange current density. Usually, the exchange current density is expressed as an Arrhenius' law function of the composition of the reacting species; however, in a recent study [1,11,15], the value of j_0 was also found to be directly proportional to the length of the TPB. It can therefore be expressed as

$$j_{0,a} = \gamma_a L_{tpb} \left(\frac{P_{H_2}}{P_{ref}}\right) \left(\frac{P_{H_2O}}{P_{ref}}\right) \exp\left(-\frac{E_{act,a}}{RT}\right) \tag{6}$$

$$j_{0,c} = \gamma_c L_{tpb} \left(\frac{P_{O_2}}{P_{ref}}\right)^{0.25} \exp\left(-\frac{E_{act,c}}{RT}\right) \tag{7}$$

where γ_a and γ_c are the coefficient for the exchange current density of the anode and the cathode, respectively, $E_{act,a}$ and $E_{act,c}$ are the activation energy at the anode and cathode, respectively, and L_{tpb} is the length of the TPB. The equation for the calculation of L_{tpb} can be expressed as [1,16,24]

$$L_{tpb} = \pi d_c N_t n_{io} n_{el} \frac{Z_{io} Z_{el}}{Z} P_{io} P_{el} \tag{8}$$

where d_c is the neck diameter of the TPB contacts (=0.26 d_{io}); Z_{io} and Z_{el} are the coordination numbers of the electronic and ionic phases, respectively; Z is the average coordination number of random packing systems of spherical particles (=6); n_{io} and n_{el} are the number fractions of the electronic-particle and ionic-particle phases, respectively; P_{io} and P_{el} are the percolation probability of the electronic and ionic phases; and N_t is the number density of all particles. The equations for solving the L_{tpb} parameters are listed in Table 1.

Table 1. Equations for solving the length of the TPB

Variable	Expression	
Coordination number of electronic phase	$Z_{el} = 3 + \frac{(Z - 3)}{n_{el} + (1 - n_{el})\beta^2}$	(9)
Coordination number of ionic phase	$Z_{io} = 3 + \frac{(Z - 3)\beta^2}{n_{el} + (1 - n_{el})\beta^2}$	(10)
Number fraction of electronic particles	$n_{el} = \frac{\alpha^3 \Phi_{el}}{1 - \Phi_{el} + \beta^3 \Phi_{el}}$	(11)
Number fraction of ionic particles	$n_{io} = 1 - n_{el}$	(12)
Percolation probability of electronic and ionic phases	$P_i = [1 - (\frac{4.236 - Z_{i-i}}{2.472})^{2.5}]^{0.4}$	(13)
Number density of all particles	$N_t = \frac{1 - \varepsilon}{(\pi / 6)d_{el}^3(n_{el} + (1 - n_{el})\beta^3)}$	(14)

3.3 Ohmic overpotential

The ohmic overpotential is an important parameter in all types of cells. The ohmic overpotential can be expressed as the following equation according to Ohm's law:

$$\eta_{ohm} = jR_{ohm} \quad (15)$$

where j is the current density, and R_{ohm} is the internal resistance of the cell, which can be estimated from the effective distance between the cell components coupled with conductivity data. According to Bossel [27], if interfacial resistances are neglected, the R_{ohm} of the cross-plane is given by

$$R_{Ohm} = \frac{\delta_{anode}}{\sigma_{anode}} + \frac{\delta_{cathode}}{\sigma_{cathode}} + \frac{\delta_{elec}}{\sigma_{elec}} \quad (16)$$

where δ_{anode} , $\delta_{cathode}$ and δ_{elec} are the thicknesses of the anode, the cathode and the electrolyte, respectively, and σ_{anode} , $\sigma_{cathode}$ and σ_{elec} are the conductivity of the anode, the cathode and the electrolyte, respectively.

3.4 Concentration overpotential

When the current is flowing and concentration gradients develop, the concentrations of species at the three-phase boundaries are different from the bulk concentrations and cause concentration losses. These losses are more pronounced when fuel or oxidant gases with low purities are fed to a fuel-cell stack. The concentration overpotential can be evaluated by the following expression:

$$\eta_{conc} = \frac{RT}{2F} \ln\left(\frac{P_{H_2OTPB} P_{H_2}}{P_{H_2O} P_{H_2TPB}}\right) + \frac{RT}{4F} \ln\left(\frac{P_{O_2}}{P_{O_2TPB}}\right) \quad (17)$$

where the first term on the right-hand side refers to the anode concentration overpotential, and the second term refers to the cathode concentration overpotential.

If the principal gaseous species in the anode are reasonably assumed to be H_2 and H_2O , those in the cathode are assumed to be O_2 and N_2 , and the external diffusion is negligible, then the relationship between the partial pressures of H_2 , H_2O , and O_2 at the three-phase boundaries are constructed:

$$P_{H_2TPB} = P_{H_2} - \frac{jRT\delta_{anode}}{2FD_{eff, anode}} \quad (18)$$

$$P_{H_2OTPB} = P_{H_2O} + \frac{jRT\delta_{anode}}{2FD_{eff, anode}} \quad (19)$$

$$P_{O_2,TPB} = P - (P - P_{O_2}) \exp\left(\frac{jRT\delta_{cathode}}{4FD_{eff,cathode}P}\right) \quad (20)$$

The effective diffusivities at the anode and cathode sides can be expressed as [1]

$$D_{eff,anode} = \left(\frac{P_{H_2O}}{P_{an}}\right)D_{H_2,eff} + \left(\frac{P_{H_2}}{P_{an}}\right)D_{H_2O,eff} \quad (21)$$

$$D_{eff,cathode} = D_{O_2,eff} \quad (22)$$

The overall effective diffusivity in a porous electrode can be expressed as [1,28]

$$D_{H_2,eff} = \frac{\varepsilon}{\tau} \left(\frac{1}{D_{H_2-H_2O}} + \frac{1}{D_{H_2,k}}\right)^{-1} \quad (23)$$

$$D_{H_2O,eff} = \frac{\varepsilon}{\tau} \left(\frac{1}{D_{H_2O-H_2}} + \frac{1}{D_{H_2O,k}}\right)^{-1} \quad (24)$$

$$D_{O_2,eff} = \frac{\varepsilon}{\tau} \left(\frac{1}{D_{O_2-N_2}} + \frac{1}{D_{O_2,k}}\right)^{-1} \quad (25)$$

The binary diffusivity is estimated using the Fuller equation [29]:

$$D_{i-j} = \frac{0.00143T^{1.75}}{pM_{ij}^{0.5}[(\sum v)_i^{1/3} + (\sum v)_j^{1/3}]^2} \quad (26)$$

where $M_{ij} = 2[(1/M_i) + (1/M_j)]^{-1}$, M is the molecular weight, and $\sum v$ is the diffusion volume (6.12 for H₂, 13.1 for H₂O, 16.3 for O₂ and 18.5 for N₂).

The Knudsen diffusivity is calculated as

$$D_{i,k} = 48.5d_p \left(\frac{T}{M_i}\right)^{0.5} \quad (27)$$

where d_p is the mean pore diameter. According to the research of Divisek et al. [25], under typical sintering conditions, the mean pore diameter is equal to the mean particle diameter. Therefore, the d_p can be reasonably set to $d_p = n_{el}d_{el} + n_{io}d_{io}$.

4. MODEL VALIDATION

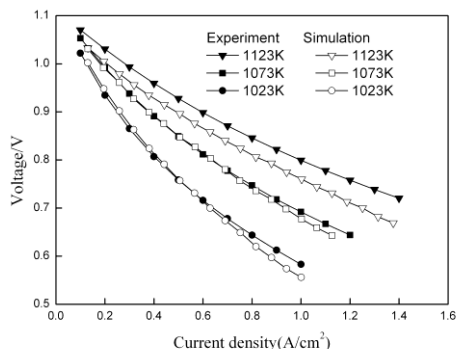


Figure 2. Comparison between experimental and simulated results

Fig. 2 shows a comparison of the model-predicted and experimental I–V curves for the SOFC. The simulation results show that the calculated polarization curves agree well with the experimental data at 1023 K and 1073 K. However, the experimental results are greater than the calculated results at 1123 K. This discrepancy might be caused by a greater effect of the ohmic heating and by a greater variation in the molar concentration along the fuel cell at higher temperatures. Nonetheless, the maximal error is less than 5%, which indicates that the model is sufficiently accurate to allow an investigation of the cell behavior. A detailed analysis of temperature effects is presented in section 5.6. Model parameters are listed in Table 2.

Table 2. Model input parameters [10,30]

Parameter	Value
Pre-exponential factor for anode, γ_a	$1.344 \times 10^{10} \text{ A m}^{-2}$
Pre-exponential factor for cathode, γ_c	$2.051 \times 10^9 \text{ A m}^{-2}$
Activation energy for anode, $E_{act,a}$	$1 \times 10^5 \text{ J mol}^{-1}$
Activation energy for cathode, $E_{act,c}$	$1.2 \times 10^5 \text{ J mol}^{-1}$
Porosity of anode and cathode, ε	0.3
Tortuosity of anode and cathode, τ	3
Conductivity of anode	$\frac{9.5 \times 10^7}{T} \exp(-\frac{1150}{T}) \text{ } \Omega\text{m}$
Conductivity of cathode	$\frac{4.2 \times 10^7}{T} \exp(-\frac{1200}{T}) \text{ } \Omega\text{m}$
Conductivity of electrolyte	$33.4 \times 10^3 \exp(-\frac{10300}{T}) \text{ } \Omega\text{m}$
Anode thickness	400 μm
Cathode thickness	10 μm
Electrolyte thickness	60 μm
Volume fraction of electronic phase, Φ_{el}	0.5
Diameter of ionic and electronic particle	1 μm

5. PARAMETRIC ANALYSIS

The validated model was used to analyze the effect of the design and operating parameters so that the performance of the cell could be improved.

5.1 Effect of the TPB length

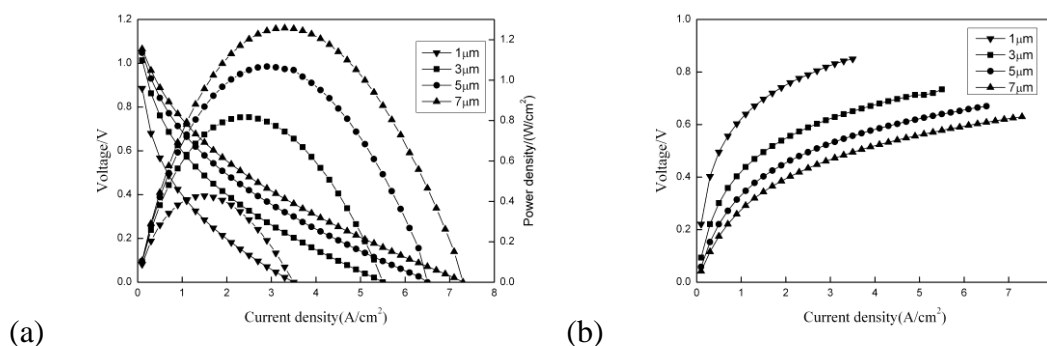


Figure 3. Effect of the TPB length: (a) I–V characteristics and power density and (b) activation overpotentials

The effects of the TPB length per contact of dissimilar particles are present in Fig. 3. For each value of TPB length, an optimum current density and, hence, a maximum power density exist. The current density that corresponds to the maximum power density shifts to higher values with increasing TPB length. Thus, the cell performance increases when the TPB length is increased. This result occurs because the electrode current density increases as the TPB length increases. The TPB length mainly influences the activation overpotential. As shown in Fig. 3b, the activation overpotential decreases significantly with increasing TPB length. The value of the TPB length is determined by the porosity, the particle diameter and the volume fraction of the electronic and ionic phases. Thus, its value can be adjusted through these parameters. The effect of particle size on the TPB length has been studied in detail by Nam et al. [16], and the effect of the volume fraction of the electronic phase on the TPB length has been studied in detail by Jeon et al. [31]; consequently, these effects were not evaluated in the course of this investigation.

5.2 The effect of porosity

In this section, the impact of the porosity on the performance is analyzed. an increase in the porosity results in a decrease in the TPB length and in an increase in the effective diffusivities; therefore, the activation overpotential increases with increasing porosity, as shown in Fig. 4b. In contrast, the concentration overpotential is decreased due to an increase in the gas diffusion rate (Fig. 4c). The combined effects result in good cell performance when the porosity is 0.2 or 0.4. However,

when the porosity reaches 0.6, the cell performance decreases significantly because of the activation overpotential. Thus, the porosity should not be greater than 0.4.

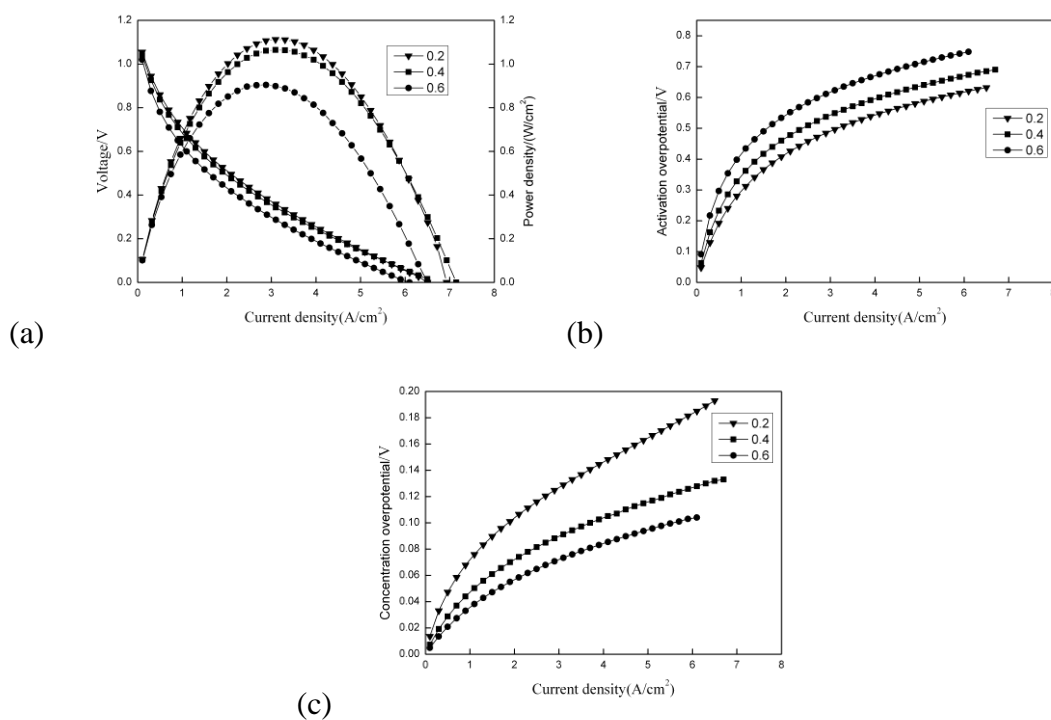


Figure 4. The effect of porosity: (a) I–V characteristics and power density, (b) activation overpotential and (c) concentration overpotential

5.3 Effect of anode thickness

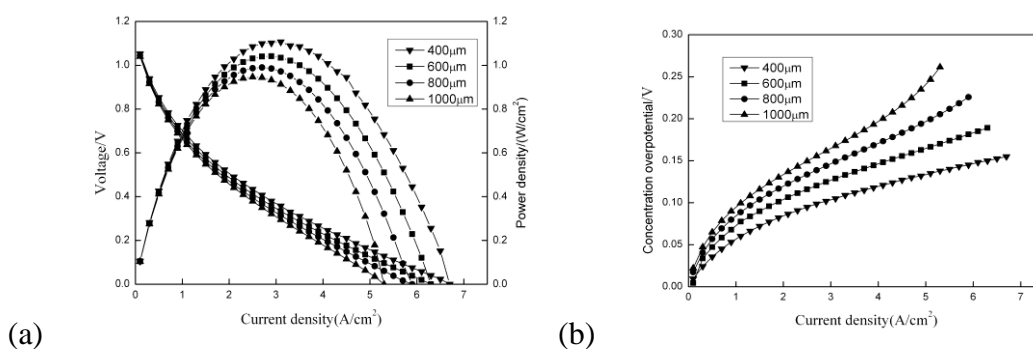


Figure 5. Effect of anode thickness: (a) I–V characteristics and power density and (b) concentration overpotential

Fig. 5a and b present the SOFC characterization curves for different anode thicknesses. Notably, the electrolyte and cathode thicknesses were fixed at 10 and 70 μm, respectively. The cell performance deteriorates with increasing anode thickness. The anode thickness influences both the

ohmic overpotential and the concentration overpotential. The ohmic concentration increases slightly with increasing anode thickness. However, the concentration overpotential increases significantly (Fig. 5b). This increase occurs because a thicker anode inhibits the diffusion of gases, which leads to a decrease in the partial pressure of H_2 at the TPB. However, the partial pressure of H_2O simultaneously increases at the TPB. As shown in Eq. (17), the concentration will consequently increase under these conditions.

5.4 The effect of electrolyte thickness

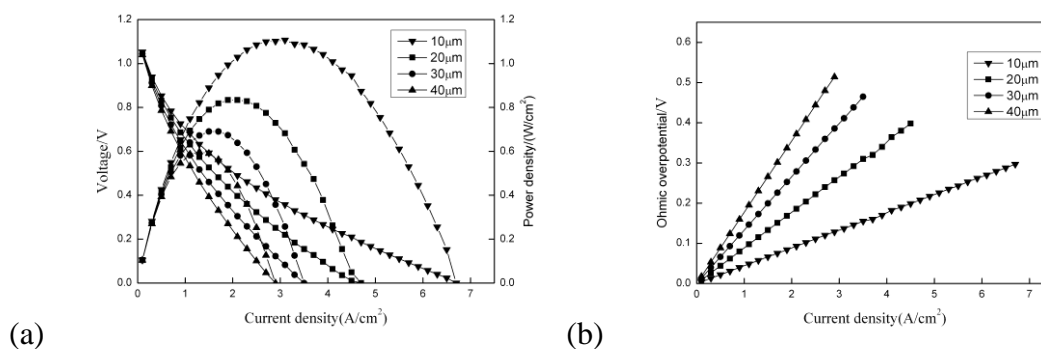


Figure 6. Effect of electrolyte thickness: (a) I–V characteristics and power density and (b) ohmic overpotential

The effect of electrolyte thickness (10, 20, 30 and 40 μm) on the performance at different current densities was investigated. As shown in Fig. 6, the performance improved significantly due to the dramatic decrease in the ohmic overpotential that resulted from the decreased electrolyte thickness. Although the ohmic overpotential was caused by the resistances of the anode, cathode and electrolyte, the effect of the anode and cathode resistances can be neglected compared to that of the electrolyte. Therefore, the ohmic overpotential of an anode-supported SOFC is smaller than that of an electrolyte-supported SOFC.

5.5 The effect of cathode thickness

The cathode thickness (40, 60, 80, and 100) was investigated at different current densities. The anode and electrolyte thickness were fixed at 400 μm and 10 μm , respectively. The results show that the cathode thickness negligibly affected the cell performance. Both the ohmic and concentration overpotentials varied slightly as the cathode thickness changed.

5.6 The effect of operating temperature

The performance of an SOFC operated at 1023 K, 1073 K and 1123 K is discussed in this section. As shown in Fig. 7a, the cell performance improved significantly due to decreases in the

activation overpotential and in the ohmic overpotential as the temperature was increased. Notably, the activation overpotential is the main voltage loss and is always greater than the ohmic overpotential because of the thin electrolyte (10 μm).

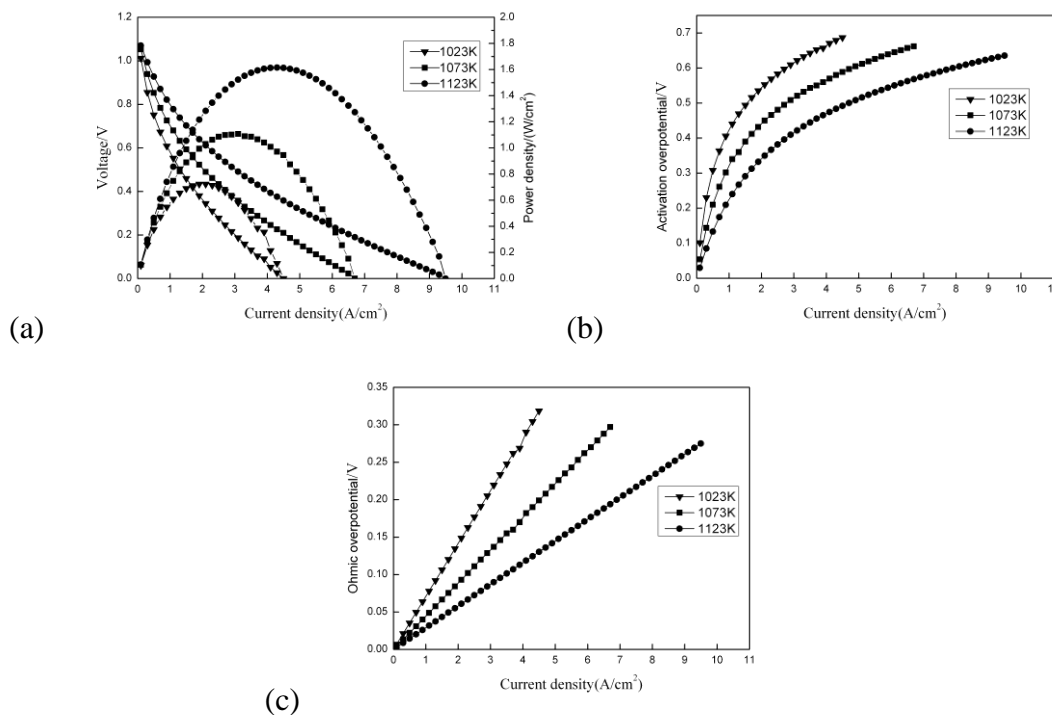


Figure 7. Effect of temperature: (a) I–V characteristics and power density, (b) activation overpotential, and (c) ohmic overpotential

In the study of Ni et al. [32], the ohmic overpotential was greater than activation overpotential at an operating temperature of 873 K and with an electrolyte thickness of 50 μm. Thus, the actual operating conditions should be considered to improve the cell performance. For this cell, the activation overpotential is the main cause of voltage loss. In contrast to the activation and ohmic overpotentials, the concentration overpotential increases as the temperature increases. However, the change is insignificant compared those induced by the activation and ohmic overpotentials. Although a decrease in the operating temperature would lead to a deterioration of the cell performance, it also would allow more common and less expensive materials to be used in the construction of certain fuel cell components [33].

5.7 The effect of operating pressure

The effect of pressure on the cell performance was also studied. The operating pressure was varied from 1 to 3 atm. As shown in Fig. 8, the cell performance decreases drastically with decreasing operating pressure. Both the activation and concentration overpotentials decrease with increasing pressure. At higher pressures, the molar fuel concentration increases at a porous electrode, and the

activation overpotential consequently decreases. The gas diffusion rate simultaneously increases, which will lead to a decrease of the concentration overpotential. The concentration overpotential is less sensitive at pressures greater than 2 atm, as evident in Fig. 8c.

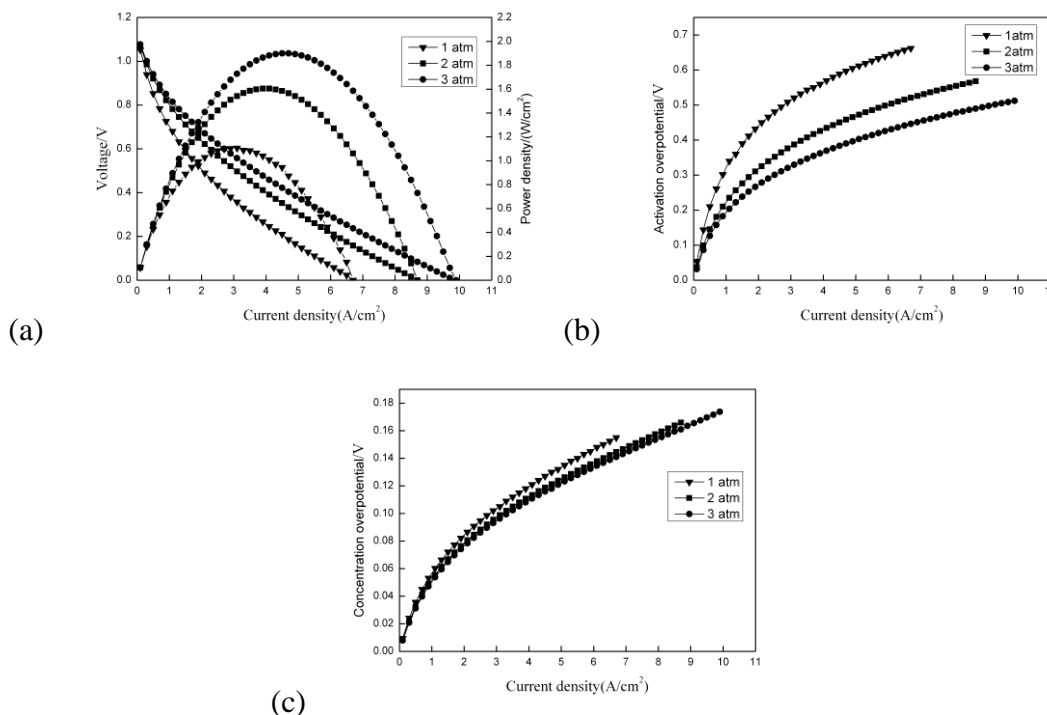


Figure 8. Effect of pressure: (a) I–V characteristics and power density, (b) activation overpotential, and (c) concentration overpotential

6. CONCLUSION

A 10×10 cm² anode-supported SOFC was tested, and the I–V curves were obtained for operating temperatures of 1023 K, 1073 K and 1123 K. An electrochemical model was subsequently built to analyze the effect of structural parameters and operating parameters on cell performance. The model was verified against experimental results for the cell.

The simulation results show that the activation overpotential dominates the performance of the cell. The ohmic overpotential is also important but is less important than the activation overpotential because of the thin electrolyte. The activation overpotential and ohmic overpotential were responsible for most of the voltage loss.

The TPB length can influence the activation overpotential significantly, and the cell performance increases substantially as the TPB length is increased. The porosity has a dual effect. When the porosity is increased, the activation increases; however, the concentration overpotential decreases. The combined effect results in good cell performance at porosity values of 0.2 and 0.4.

The electrolyte thickness is the dominant factor with respect to ohmic overpotential. Compared to the effects of the electrolyte thickness, the effects of the anode and cathode thicknesses on the ohmic

overpotential can be neglected. Anode thickness mainly influences the concentration overpotential. Decreased electrolyte and anode thicknesses can improve the cell performance.

Increases in the operating temperature and pressure results in decreases in the activation and concentration overpotentials, which, in turn, results in enhanced cell performance.

References

1. S. H. Chan and Z. T. Xia, *J. Electrochem. Soc.*, 148(2001)388.
2. F. Ishak, I. Dincer and C. Zamfirescu, *J. Power Sources*, 212(2012)73.
3. R. Bove, P. Lunghi and N. M. Sammes, *Int. J. Hydrogen Energ.*, 30(2005)181.
4. R. Bove, P. Lunghi and N. M. Sammes, *Int. J. Hydrogen Energ.*, 30(2005)189.
5. W. Zhang, E. Croiset, P.L. Douglas, M.W. Fowler and E. Entchev, *Energy Convers. Manage.*, 46(2005)181.
6. A. O. Omosun, A. Bauen, N. P. Brandon, C. S. Adjiman and D. Hart. *J. Power Sources*, 131(2004) 96.
7. Y. Inui, A. Urata, N. Ito, T. Nakajima and T. Tanaka, *Energy Convers. Manage.*, 47 (2006) 1738.
8. S. H. Chan, H. K. Ho and Y. Tian, *Int. J. Hydrogen Energ.*, 28(2003) 889.
9. S. C. Singhal, *Solid State Ion.*, 135(2000) 305.
10. M. M. Hussain, X. Li and I. Dincer, *J. Power Sources*, 189(2009)916.
11. M. Ni, M. K. H. Leung and D. Y. C. Leung, *Energy Convers. Manage.*, 48(2007)1525.
12. V. M. Janardhanan, V. Heuveline and O. Deutschmann, *J. Power Sources*, 178 (2008)368.
13. Y. B. Kim, C. Chao, T. M. Gur, and F. B. Prinz, *ECS Transactions*, 25 (2009) 917.
14. X. Deng and A. Petric, *J. Power Sources*, 140(2005) 297.
15. S. H. Chan, X. J. Chen and K. A. Khor, *J. Electrochem. Soc.*, 151(2004) 164.
16. J. H. Nam and D. H. Jeon, *Electrochim. Acta.*, 51(2006) 3446.
17. P. Costamagna, L. Magistri and A. F. Massardo, *J. Power Sources*, 96(2001) 352.
18. M. Andersson, J. Yuan and B. Sundén, *Int. J. Heat Mass Tran.*, 55(2012)773.
19. L. Petruzzi, S. Cocchi and F. Fineschi, *J. Power Sources*, 118(2003) 96.
20. Y. Shi, N. Cai, C. Li, C. Bao, E. Croiset, J. Qian, Q. Hu and S. Wang, *J. Power Sources*, 172(2007) 235.
21. Y. Patcharavorachot, A. Arpornwichanop and A. Chuachuensuk, *J. Power Sources*, 177 (2008)254.
22. T. S. Li, H. Miao, T. Chen, W. G. Wang, and C. Xu, *J. Electrochem. Soc.*, 156 (2009)1383.
23. T. S. Li, W. G. Wang, H. Miao, T. Chen and C. Xu, *J. Alloys. Compd.*, 495 (2010) 138.
24. S. H. Chan, X. J. Chen and K. A. Khor, *J. Electrochem. Soc.*, 151(2004)164.
25. J. Divesek, R. Wilkenhoner and Y. volfkovich, *J. Appl. Electrochem.*, 29(1999) 153.
26. D. A. Noren and M. A. Hoffman, *J. Power Sources*, 152(2005)175.
27. U.G. Bossel, *Final Report on SOFC data facts and figures*, Swiss Federal Office of Energy, Berne(1992).
28. P. Costamagna and A. Selimovic, *Chem. Eng. J.*, 102(2004)61.
29. B. E. Poling, J. M. Prausnitz and J. P. Oconnell, *The Properties of Gases and Liquids*, 5th ed., McGraw-Hill, New York(2001).
30. S. Campanari and P. lora, *Fuel Cell* 5(2005)34.
31. D. H. Jeon, J. H. Nam and C.J. Kim, *J. Power Sources*, 139 (2005) 21.
32. M. Ni, M. K. H. Leung and Dennis Y. C. Leung, *Energy Convers. Manage.*, 48(2007)1525.
33. S. M. Haile, *Acta Mater.*, 51(2003)5981.

Nomenclature:

E = activation energy, J mol^{-1}

F = Faraday's constant, $96485.34 \text{ C mol}^{-1}$

L_{tpb} = length of TPB, m/m^3

M = molecular weight, kg kmol^{-1}

P = pressure, bar

R = universal gas constant, $8.314 \text{ J mol}^{-1}\text{K}^{-1}$

T = temperature, K

V = voltage, V

Z = Coordination number

d = diameter, m

j_0 = exchange current density, A m^{-2}

j = electric current density, A m^{-2}

Φ = volume fraction

α = symmetrical coefficient

β = size ratio of ionic particles to electronic particles

γ = pre-exponential factor for exchange current density, A m^{-2}

δ = thickness, m

σ = conductivity, Ωm

ε = porosity

τ = tortuosity

η = polarization loss, V